frontiers | Frontiers in Energy Research

TYPE Original Research
PUBLISHED 17 January 2023
DOI 10.3389/fenrg.2022.995800

OPEN ACCESS

EDITED BY
David J. Heldebrant,
Pacific Northwest National Laboratory (DOE), United States

REVIEWED BY
Song Yang,
Guizhou University, China
Guoliang Liu,
Wuhan University, China

*CORRESPONDENCE
Chunshan Song,
chunshansong@cuhk.edu.hk
Xinwen Guo,
guoxw@dlut.edu.cn

SPECIALTY SECTION
This article was submitted to Carbon Capture, Utilization and Storage, a section of the journal Frontiers in Energy Research

RECEIVED 16 July 2022
ACCEPTED 09 November 2022
PUBLISHED 17 January 2023

CITATION
Huang J, Zhang G, Wang M, Zhu J, Ding F, Song C and Guo X (2023), The synthesis of higher alcohols from CO_2 hydrogenation over Mn-Cu-K modified Fe_5C_2 and CuZnAlZr tandem catalysts. *Front. Energy Res.* 10:995800. doi: 10.3389/fenrg.2022.995800

The synthesis of higher alcohols from CO_2 hydrogenation over Mn-Cu-K modified Fe_5C_2 and CuZnAlZr tandem catalysts

Jiamin Huang[1], Guanghui Zhang[1], Mingrui Wang[1], Jie Zhu[1], Fanshu Ding[1], Chunshan Song[1,2]* and Xinwen Guo[1]*

[1]State Key Laboratory of Fine Chemicals, PSU-DUT Joint Center for Energy Research, School of Chemical Engineering, Dalian University of Technology, Dalian, China, [2]Department of Chemistry, Faculty of Science, The Chinese University of Hong Kong, Shatin, China

The catalytic production of higher alcohols (HAs) is a promising path for converting CO_2 into value-added chemical products. The application is still limited by the low selectivity of HAs (less than 10%) on most catalysts. Here, we report a tandem catalyst consisting of Mn-Cu-K modified iron carbide and CuZnAlZr catalyst. The modification of iron carbide with Mn, Cu and K promoters improves the formation of HAs (13.5% Sel.), and the construction of tandem catalysts with CuZnAlZr can further enhance the catalytic performance. By examining different catalyst filling methods and the filling ratio of the tandem catalyst, it was found that the powder mixing resulted in a higher selectivity of HAs with a mass ratio of the two components of 1:1, and a synergistic effect leads to a higher selectivity of HAs (15.5%) with about 40% of propanol and butanol among HAs.

KEYWORDS

CO_2 hydrogenation, higher alcohols, tandem catalyst, modified iron carbide, CuZnAlZr catalyst

1 Introduction

The increase in global CO_2 emissions has led to a gradual increase in atmospheric CO_2 concentration, which has been linked to a series of environmental problems such as global climate change, melting glaciers and rising sea levels. As a part of an integrated solution (including the increased use of renewable energy, CO_2 capture, utilization and storage), catalytic conversion of CO_2 into chemicals with added value, such as methanol, lower olefins and liquid fuels, can not only reduce the CO_2 concentration, but also relieve the dependence on fossil fuels (Liang et al., 2019; Tada et al., 2019; Gao et al., 2020; Temvuttirojn et al., 2020; Wu et al., 2021) In recent years, there has been significant interest in the hydrogenation of CO_2 into HAs (represents ethanol and alcohols with carbon number above 2 such as propanol and butanol). This is because higher alcohols require catalysts with both the ability to form oxygenated compounds and the ability to grow carbon chains compared to methanol, and alcohol products with long carbon chains have higher industrial applications (Luk et al., 2017; Zeng et al., 2021) HAs is widely used

as fuels and solvents in industry and consumed in large quantities each year, and the demand for HAs is likely to increase significantly in the future given the rapid growth in the world's demand for chemicals and fuels.

HAs are mainly produced through the hydration of petroleum-derived olefins and the fermentation of starch. However, these methods are agriculture-dependent and have low productivity. Therefore, it is necessary to develop new and efficient methods to produce HAs (Xu et al., 2020a) At present, much progress has been made in the hydrogenation of CO_2 to methanol, and a few catalysts have been applied in industrial scale applications (Behrens et al., 2012; Temvuttirojn et al., 2020) However, direct conversion of CO_2 to HAs is currently still a grand challenge (Zhao et al., 2018; Nie et al., 2019; Yang et al., 2019; Zhang et al., 2021) Most studies on CO_2 hydrogenation to HAs focused on modified Fischer-Tropsch Synthesis (FTS) catalysts (Fe and Co catalysts), modified methanol synthesis catalysts (Cu-based catalysts) and Rh-based catalysts, etc. (Ning et al., 2016; Luk et al., 2017; Zhao et al., 2017; Ao et al., 2018; Cao et al., 2018) The synthesis of HAs requires rationally designed catalysts to promote the growth of carbon chains and to accelerate the insertion of oxygen-containing intermediates (e.g., CHO*, CO) into the carbon chains (Yang et al., 2019; Zhang et al., 2021)

Fe-based catalysts have recently been extensively studied in the production of hydrocarbons via CO_2 hydrogenation (Liu et al., 2018; Liu et al., 2019; Liu et al., 2020; Zhu et al., 2020; Zhu et al., 2022), and Fe_5C_2 is essential for carbon chain growth (Liu et al., 2021) Iron carbide has moderate chain growth ability, higher activity and lower cost than Co and Ce based catalysts, so it is commonly used for CO_2/CO hydrogenation to produce C_2~C_4 hydrocarbons. Fe-Mn catalyst is active for the hydrogenation of CO_2 to HAs, and Mn is usually used as a structural as well as electronic promoter, which can improve the ability of CO insertion (Kangvansura et al., 2016; Yang et al., 2018; Nie et al., 2019) Martin et al. reported a K/Mn/Fe/NCNT catalyst for CO_2 hydrogenation, where alcohols were observed in products containing methanol and ethanol (8.4% in total), but not in products with longer carbon chains (Kangvansura et al., 2016; Kangvansura et al., 2017) In addition, Fe-Cu catalyst has been used for the production of HAs from syngas with high activity. Metallic Cu is responsible for the adsorption and insertion of non-dissociated CO, and the FeC_x-Cu interface promotes the formation of HAs (Xu et al., 2020a; Xu et al., 2020b) Alkali metals such as Na, K and Cs are widely used as promoters, and they can inhibit the further hydrogenation of the adsorbed C_xH_y intermediates, providing more opportunities for the formation of higher alcohols and olefins (Iranmahboob et al., 2003; Tienthao et al., 2007; Christensen et al., 2009; Cosultchi et al., 2012; Portillo Crespo et al., 2015; Xu et al., 2020a) Furthermore, alkali promoters can also promote the formation and stabilization of Fe_5C_2, facilitating the chain growth (Xu et al., 2020b) Besides, Liu et al. reported a tandem catalyst composed of CuZnAl and K-CuMgZnFe for the synthesis of HAs in CO_2 hydrogenation, and the proper proximity of the two components accelerates the transfer of CO* intermediates from CuZnAl to K-CuMgZnFe (Xu et al., 2021) Wang et al. reported a Na-Fe@C catalyst and demonstrated that oxygen-containing compounds can effectively migrate at the interface of Fe_5C_2 as well as CuZnAl oxides, which further promotes the formation of higher alcohols. Therefore, we speculate that the modified iron carbide catalyst in our work is equally capable of species migration with the CuZnAlZr catalyst, leading to the improvement of the selectivity of higher alcohols (Wang et al., 2021) Sun et al. reported a CoMn/CuZnAlZr catalyst for the preparation of HAs, where the CuZnAlZr catalyst can effectively promote the formation of CH_xO* intermediates, and the abundant CH_xO* intermediates participate in the subsequent HAs formation. Therefore, we prepared a similar CuZnAlZr catalyst and tested it in tandem with our MnCuK-FeC catalyst (Lin et al., 2019)

In this work, Mn, Cu and K were used to modify iron carbide and enhance its ability to produce more HAs. A CuZnAlZr catalyst was prepared and coupled with Mn-Cu-K modified iron carbide for CO_2 hydrogenation. By testing different catalyst filling methods and filling mass ratios, it was found that the catalysts performed best when mixed with 1:1 powder, and the selectivity of HAs in the total product reached 15.5%.

2 Experimental section

2.1 Materials and methods

Ferrous oxalate (Aladdin Chemicals, >99%), aqueous manganese nitrate (Aladdin Chemicals, 50%), copper nitrate ($Cu(NO_3)_2{\cdot}6H_2O$, Aladdin Chemicals, >99%), potassium nitrate (Aladdin Chemicals, >99%), zinc nitrate ($Zn(NO_3)_2{\cdot}6H_2O$, Aladdin Chemicals, >99%), aluminum nitrate ($Al(NO_3)_3{\cdot}9H_2O$, zirconium nitrate ($Zr(NO_3)_4{\cdot}5H_2O$, Aladdin Chemicals, >99%), anhydrous sodium carbonate (Aladdin Chemicals, >99%).

2.2 Catalyst preparation

Mn-Cu-K modified iron carbide catalysts were prepared by a previously reported method (Liu et al., 2021) Typically, 2.0 g of ferrous oxalate, 0.65 g of aqueous manganese nitrate, 0.38 g of copper nitrate and 0.06 g of potassium nitrate were mixed at room temperature. The obtained composite was kept at room temperature for 48 h and then dried at 60°C for 24 h. The obtained powder was then placed in a tube furnace and heated to 350°C at 0.45°C/min under a 10% CO-N_2 atmosphere, and then carburized for 4 h. After natural cooling of the catalyst to room temperature, the gas was switched to 1%

O_2-N_2 for 24 h to passivate it. The product is denoted as MnCuK-FeC. The unmodified FeC catalyst was prepared in a similar way without the introduction of any other promoters.

CuZnAlZr catalyst was prepared by a previously reported co-precipitation method (Lin et al., 2019) 9.66 g of copper nitrate, 3.79 g of zinc nitrate, 7.51 g of aluminum nitrate, and 0.86 g of zirconium nitrate were dissolved in 40 ml of deionized water. Next, 12.72 g of anhydrous sodium carbonate was subsequently weighed and dissolved in 60 ml of deionized water. The above two solutions were slowly added dropwise to a beaker containing 200 ml of deionized water at a controlled temperature of 30°C and a pH of 8.0. After stirring at 30°C for 3 h, the resulting suspension was centrifuged, washed, and dried at 80°C for 24 h. Finally, the dried product was calcined in a muffle furnace at 350°C with a heating rate of 5°C/min for 4 h to obtain the CuZnAlZr catalyst. The subsequent catalyst composed with MnCuK-FeC and CuZnAlZr (mass ratio = 1:1) was named as MnCuK-FeC/CuZnAlZr.

2.3 Catalyst characterization

X-ray diffraction (XRD) patterns were obtained on a Rigaku SmartLab diffractometer with Cu Kα radiation (λ = 1.5406 Å) at a scan rate of 8°/min. The 2θ degree range was from 10° to 80°. *In-situ* XRD experiments were conducted with an XRK 900 reaction chamber manufactured by Anton Paar to track the phase transition. Typically, 60 mg of catalyst was loaded into a gas-tight chamber and pre-carburized in pure CO at 350°C and ambient pressure. After the sample was cooled to 300°C, the feed gas was switched to the reaction gas (CO_2:H_2:N_2 = 21:63:16) at a rate of 30 ml/min and the reaction pressure was maintained at 0.8 MPa.

CO_2-temperature programmed desorption (TPD) was measured using a Quantachrome ChenBETPulsar analyzer. Approximately 120 mg of passivated catalyst was loaded and pretreated with 10% H_2-Ar for 25 min at 400°C to remove the surface passivated layer. The gas was then switched to CO_2 for 1 h at room temperature to achieve saturated adsorption. The atmosphere was changed to He to start the analysis procedure, and the sample was then heated to 700°C at 10°C/min.

We obtained *in-situ* diffuse reflectance infrared Fourier transform (DRIFT) spectra on a Thermo Nicolet™ iS™50 spectrometer with a liquid nitrogen-cooled mercury cadmium telluride (MCT) detector. Before testing, we pretreated samples with 10% CO-N_2 at 350°C and ambient pressure for 1 h, and then samples were purged with N_2 and cooled to 300°C and the background was collected. The reactant gas (CO_2: H_2 = 1:3) was fed to the samples at 300°C and 1 MPa, then the spectra were subsequently obtained.

Fourier Transform Infrared spectroscopy (FT-IR) measurements were carried out on a Thermo Scientific Nicolet™ iS™50 spectrometer. The spectra were collected from 500 to 4000 cm^{-1} with a resolution of 4 cm^{-1}.

Micro Confocal Raman Spectroscopy measurements were carried out on a Invia Qontor spectrometer. The spectra were collected from 200 to 2000 cm^{-1} with a 532 nm laser.

High resolution transmission electron microscopy (HRTEM) was performed on an FEI Tecnai F30 instrument. The sample was dispersed in ethanol and the suspended solution was dropped on a copper grid before imaging.

X-ray photoelectron spectroscopy (XPS) analysis was performed by a spectrometer (Model Max 200, Leybold, Germany) using Al Kα radiation as the source of excitation.

Energy dispersive spectroscopy (EDS) mapping and scanning transmission electron microscopy (STEM) images were obtained on an F200 field emission transmission electron microscope with a voltage of 200 kV.

The ^{57}Fe Mössbauer spectra was measured on a Topologic 500A spectrometer at room temperature. The emission source was ^{57}Co (Rh) constant-motion acceleration mode, and the spectra were analyzed using a Lorentzian line shape for fold fitting.

2.4 Catalyst testing

The CO_2 hydrogenation reaction was carried out in a fixed bed reactor. 0.2 g of the catalyst as well as 0.5 g of quartz sand were loaded. Before testing, the catalyst was pre-carburized in a pure CO stream (15 ml/min) at 350°C and ambient pressure for 1 h. The gas was then switched from CO to N_2 for purging. After the temperature was lowered to 300°C, the reaction gas (T = 300°C, p = 3 MPa, CO_2:H_2:N_2=21:63:16, 6000 ml h^{-1}·g_{cat}^{-1}) was fed. The products were analyzed using an on-line gas chromatograph, model Agilent 7890B, with a thermal conductivity detector (TCD) for N_2, CO, CO_2 and CH_4, and a flame ionization detector (FID) for hydrocarbon and alcohol products.

CO_2 conversion rate and product selectivity are calculated by the following Eqs. 1–9:

$$\mathrm{CO_2\ Conversion} = \frac{nCO_{2,in} - nCO_{2,out}}{nCO_{2,in}} \times 100\% \quad (1)$$

$$\mathrm{CO\ Selectivity} = \frac{nCO}{nCO + \sum i \times nC_iH_x + \sum i \times nC_iH_xO} \times 100\% \quad (2)$$

$$\mathrm{CH\ Selectivity} = \frac{\sum i \times nC_iH_x}{nCO + \sum i \times nC_iH_x + \sum i \times nC_iH_xO} \times 100\% \quad (3)$$

$$\mathrm{MeOH\ Selectivity} = \frac{nCH_3OH}{nCO + \sum i \times nC_iH_x + \sum i \times nC_iH_xO} \times 100\% \quad (4)$$

$$\mathrm{EtOH\ Selectivity} = \frac{2nC_2H_5OH}{nCO + \sum i \times nC_iH_x + \sum i \times nC_iH_xO} \times 100\% \quad (5)$$

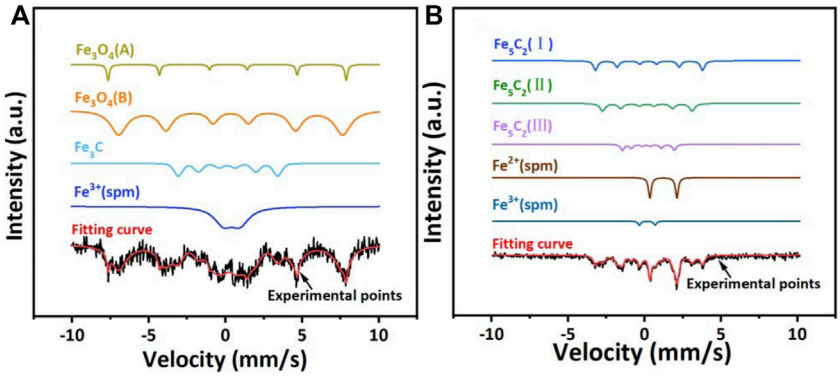

FIGURE 1
Mössbauer spectra of the **(A)** passivated MnCuK-FeC **(B)** spent MnCuK-FeC.

$$\text{PrOH Selectivity} = \frac{3nC_3H_7OH}{nCO + \sum i \times nC_iH_x + \sum i \times nC_iH_xO} \times 100\% \quad (6)$$

$$\text{BuOH Selectivity} = \frac{4nC_4H_9OH}{nCO + \sum i \times nC_iH_x + \sum i \times nC_iH_xO} \times 100\% \quad (7)$$

$$\text{HAs Selectivity} = \frac{\sum i \times nC_iH_xO - nCH_3OH}{nCO + \sum i \times nC_iH_x + \sum i \times nC_iH_xO} \times 100\% \quad (8)$$

$$\text{HAs}\Big/\text{ROH} = \frac{2nC_2H_5OH + 3nC_3H_7OH + 4nC_4H_9OH}{nCH_3OH + 2nC_2H_5OH + 3nC_3H_7OH + 4nC_4H_9OH} \times 100\% \quad (9)$$

The CH represents all hydrocarbon products. The $nCO_{2,in}$ and $nCO_{2,out}$ represent the CO_2 in feed and effluent molar concentration, respectively; nCO represents the molar concentration of effluent CO; nC_iH_x represents the molar concentration of effluent hydrocarbons corresponding to i carbon number; nCH_3OH, nC_2H_5OH, nC_3H_7OH, nC_4H_9OH represents the molar concentration of effluent CH_3OH, C_2H_5OH, C_3H_7OH, C_4H_9OH, respectively; nC_iH_xO represents the molar concentration of effluent alcohol products corresponding to i carbon number; i represent the number of carbons. $\sum i \times nC_iH_x$ represents the molar concentration of all effluent hydrocarbon products; $\sum i \times nC_iH_xO$ represents the molar concentration of all effluent alcohol products.

3 Results and discussion

3.1 The structural characterization of catalysts

The XRD pattern of the passivated MnCuK-FeC catalyst (Supplementary Figure S1A) shows the characteristic reflections of Fe_3O_4 (JCPDS, no. 19–0629) at 35.3°, 42.9°, 56.9°, and 62.4°. The XRD and ^{57}Fe Mössbauer spectra (Figure 1A and Table 1A) indicated that the catalyst composition was mainly Fe_3O_4. The XPS results in Supplementary Figure S2 show that the catalyst surface contains Fe_3O_4, MnO, CuO, but only Fe_3O_4 was observed in the XRD results, possibly owing to the high dispersion of Mn and Cu (Supplementary Figure S10A) (Xu et al., 2020b) The XRD pattern of CuZnAlZr catalyst is shown in Supplementary Figure S1B and the catalyst showed characteristic diffraction peaks of CuO at 35.3°, 38.8° and 48.1°, but no other species was observed, consistent with the high content of Cu in the catalyst. Therefore, in order to further investigate the composition of the two catalysts, FT-IR and Raman tests were performed to determine the composition of the two catalysts, and the results obtained were compared with those in the literature. The results are shown in Supplementary Figures S4 and S5. The MnCuK-FeC catalyst shows signals of Fe_5C_2, MnO and CuO in the Raman spectra, while the CuZnAlZr catalyst shows signals of the four metal oxides (CuO, ZnO, Al_2O_3, ZrO_2), which corresponds to the XPS results in Supplementary Figure S3 (Zhuo et al., 2008; Ahmed et al., 2013; Liu et al., 2014a; Bauer, 2018; Mironova-Ulmane et al., 2018; Lee et al., 2021) Besides, the FT-IR results also show the chemical bonds contained in the two catalysts (Zheng et al., 2013; Jayarambabu, 2014; Elango et al., 2017; Naayi et al., 2018; Chang et al., 2022)

The passivated MnCuK-FeC catalyst was pretreated by CO prior to the catalytic reactions, and *in-situ* XRD was performed to track the structural evolution (Figure 2A). Under CO treatment, the reflections of Fe_3O_4 rapidly disappeared at 350°C and the reflections of Fe_5C_2 became more intense, suggesting the transition from Fe_3O_4 to Fe_5C_2. The formation of Fe_5C_2 is corroborated by the result of the spent MnCuK-FeC catalyst Mössbauer spectra (Table 1B). Meanwhile, the CuO in the catalyst was also reduced, the reflections of metallic Cu

TABLE 1 Mössbauer parameters of catalysts.

Catalyst	Assignment	Is	Qs	H	Spectral Contribution (%)
MnCuK-FeC (Passivated)	Fe_3O_4(A)	0.14	−0.07	48.2	6.16
	Fe_3O_4(B)	0.34	–	453.9	58.8
	Fe_3C	0.13	0.05	20.1	13.19
	Fe^{3+}(spm)	0.4	1.07	–	21.85
MnCuK-FeC (Spent)	χ-Fe_5C_2 (I)	0.26	0.06	21.8	29.25
	χ-Fe_5C_2 (II)	0.16	0.05	18.2	29.25
	χ-Fe_5C_2 (III)	0.18	0.14	10.5	16.14
	Fe^{2+}(spm)	1.23	1.77	–	21.2
	Fe^{3+}(spm)	0.17	1.04	–	4.16

IS, Isomer shift; QS, Q. Splitting; H, Magnetic field.

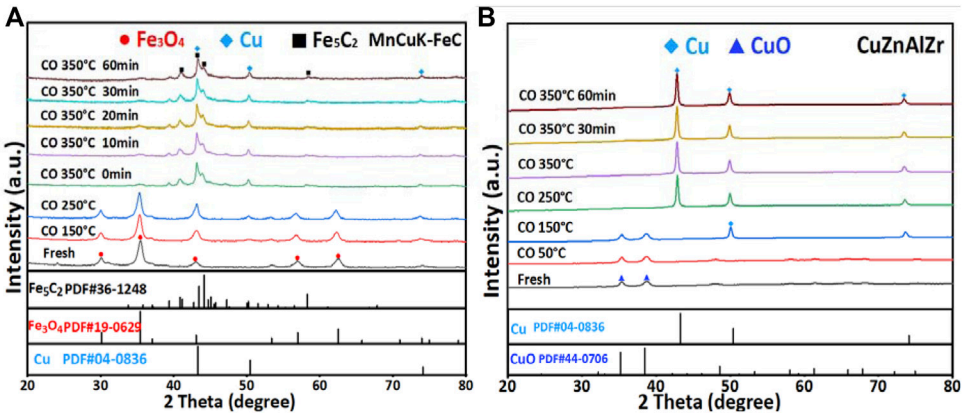

FIGURE 2
In-situ XRD patterns during CO treatment of **(A)** MnCuK-FeC catalyst and **(B)** CuZnAlZr catalyst.

appeared at 43.3°, 50.5° and 73.9° after the temperature raised to 250 °C. The reflections of Fe_3O_4 disappeared after 60 min of CO treatment at 350°C, suggesting a full carburization. For CuZnAlZr (Figure 2B), the reflections of CuO disappeared rapidly at 250°C under CO atmosphere, and the diffractions of metallic Cu appeared, indicating that CuO in CuZnAlZr catalyst was quickly reduced to Cu^0. These results are consistent with the CO *in-situ* XRD results of MnCuK-FeC/CuZnAlZr mixed catalyst (Figure 3), which showed reflections of metallic Cu after the CO pretreatment.

3.2 Catalytic performance of CO_2 hydrogenation

We first investigated the catalytic performance of the unmodified iron carbide (XRD result in Supplementary Figure S6). As shown in our previous work, we can see that the unmodified iron carbide showed the high hydrocarbon selectivity (94.2%) and low CO selectivity (5.6%) (Huang et al., 2022), with almost no alcohols in the products (Table 2). This indicates that the catalyst has a strong capacity on the production of hydrocarbons, while the non-dissociative activation of CO is poor and the insertion of CO into the carbon chain is restricted to form HAs. Therefore, we added Mn and Cu to iron carbide to enhance its non-dissociative activation of CO and promote the formation of HAs (Kangvansura et al., 2016; Xu et al., 2020b) Besides, alkali promoter K was introduced to increase the C/H ratio on the catalyst surface to inhibit deep hydrogenation (Iranmahboob et al., 2003; Cosultchi et al., 2012; Liu et al., 2014b) As shown in Figure 4, no desorption peak of CO_2 was observed in the MnCu-FeC, while a strong desorption peak appeared between 500°C and 650°C after the addition of 1 wt% K. This indicates that an increased adsorption of CO_2 on

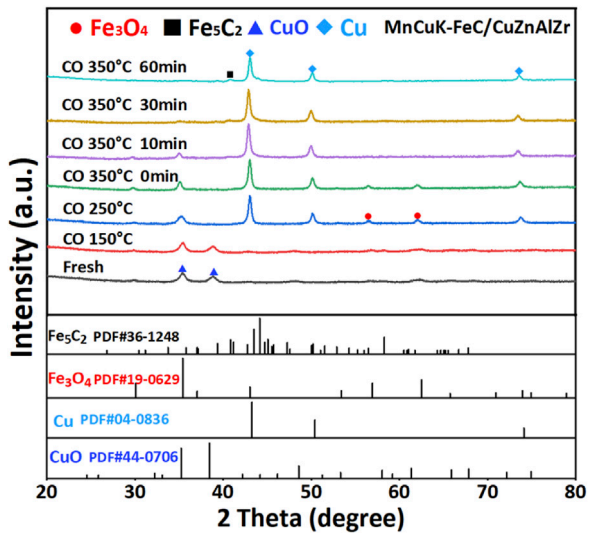

FIGURE 3
In-situ XRD patterns during CO treatment of the MnCuK-FeC/CuZnAlZr catalyst.

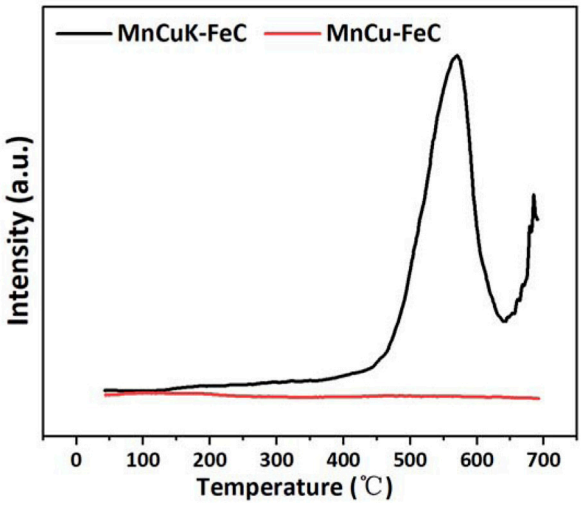

FIGURE 4
CO_2-TPD profiles of the catalysts MnCuK-FeC and MnCu-FeC.

TABLE 2 CO_2 hydrogenation performance over the FeC-based catalysts and tandem catalysts.

Catalyst	CO_2	Sel. (%)						HAs/ROH
	Conv. (%)	CO	CH[a]	MeOH[b]	EtOH[c]	PrOH[d]	BuOH[e]	(Mol%)
[f]FeC Huang et al. (2022)	38.3	5.6	94.2	0.2	0	0	0	0
MnCuK-FeC	40.8	26.6	58.7	1.2	8.8	3.5	1.2	91.8
CuZnAlZr	28.1	91.3	0.5	8.2	0	0	0	0
MnCuK-FeC(1)/ CuZnAlZr(1) dual bed-a	38.5	23.8	62.1	1.1	8.1	3.2	1.7	92.2
MnCuK-FeC(1)/ CuZnAlZr(1) dual bed-b	38.9	24.2	61.7	3.6	7.1	2.3	1.1	74.5
MnCuK-FeC(1)/ CuZnAlZr(1)	42.1 33.2	22.7	60.6	1.2	9.3	4.0	2.2	92.8
MnCuK-FeC(1)/ CuZnAlZr(2)		40.6	48.2	3.6	5.3	1.5	0.8	67.9
MnCuK-FeC(2)/ CuZnAlZr(1)	36.8	24.9	61.7	1.5	7.4	2.9	1.6	88.8

Reaction conditions: 300°C, 3 MPa, 6000 ml h^{-1}·$gcat^{-1}$, H_2:CO_2=3:1
a all hydrocarbon products. b methanol. c ethanol. d propanol. e butanol
f data from our previous work
MnCuK-FeC(1)/CuZnAlZr(2) means the two catalysts are mixed in powder with a mass ratio of 1:2
MnCuK-FeC(1)/CuZnAlZr(1) means the two catalysts are mixed in powder with a mass ratio of 1:1
MnCuK-FeC(2)/CuZnAlZr(1) means the two catalysts are mixed in powder with a mass ratio of 2:1
Conv., Conversion; Sel., Selectivity

the catalyst surface, inhibiting the deep hydrogenation of CH products. And it is reported that the unsaturated carbon chains were more conducive to the insertion of CO, thus accelerating the formation of HAs (Tienthao et al., 2007; Christensen et al., 2009) Therefore, we added Mn, Cu, and K to the iron carbide with an appropriate ratio, which was used to enhance the non-dissociated CO activation and inhibit deep hydrogenation of the catalyst. The MnCuK-modified iron carbide catalyst was evaluated for CO_2 hydrogenation. It was found that the product distribution exhibits a significant change. More HAs (13.5% in total products)

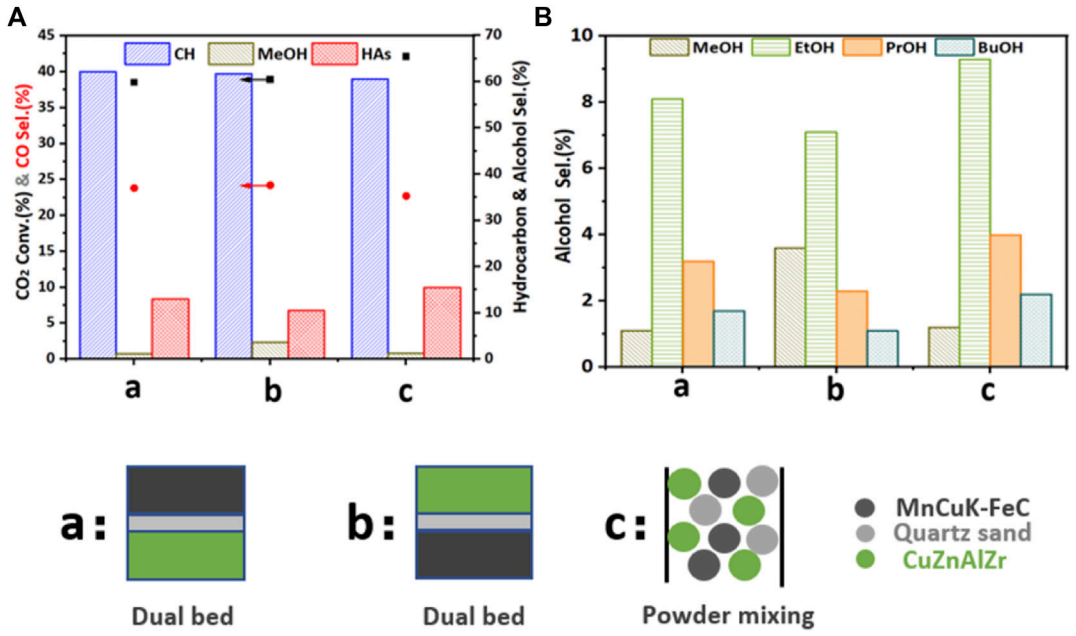

FIGURE 5
Results of CO_2 hydrogenation performed on different catalyst filling methods. **(A)** CO_2 conversion and selectivity of CH, MeOH, HAs and CO. **(B)** Selective distribution of different alcohol products. (The mass ratio of MnCuK-FeC and CuZnAlZr in different filling methods is 1:1) Reaction conditions: 3 MPa, 300°C, 6000 ml $h^{-1}{\cdot}g_{cat}^{-1}$, H_2:CO_2 = 3:1.

were generated while the proportion of propanol and butanol reached 35% in the alcohols (Table 2). This result is consistent with our expectation that the collective addition of MnCuK into iron carbide can substantially promote the non-dissociative activation of CO and favor the generation of oxygenated compounds, especially HAs products.

Next, we tested the single CuZnAlZr catalyst for CO_2 hydrogenation, and the results showed that the CuZnAlZr catalyst exhibited high reverse water gas shift (RWGS) performance, which is consistent with the similar results reported in the literature (Lin et al., 2019) In this work, Mn, Cu and K were used to modify iron carbide and enhance its ability to produce more HAs. A CuZnAlZr catalyst was prepared and coupled with Mn-Cu-K modified iron carbide for CO_2 hydrogenation. By testing different catalyst filling methods and filling mass ratios, it was found that the catalysts performed best when mixed with 1:1 powder, and the selectivity of HAs in the total product reached 15.5%

3.3 The effect of the proximity in the tandem catalyst

We investigated the proximity of MnCuK-FeC and CuZnAlZr by comparing different catalyst loading methods. The mass ratio of MnCuK-FeC and CuZnAlZr was fixed at 1:1. As shown in Figures 5A,B, for the dual-bed configuration (models a and b), the conversion of CO_2 was 38.5% and 38.9%, and the selectivity of HAs was 13.0% and 10.5%, respectively (Table 2), suggesting that different catalyst loading methods have a significant effect on the selectivity of HAs. Therefore, we loaded the two catalysts with a powder mixture, and the results in Table 2 show that powder mixing-filling method (Figure 5C) can further improve the selectivity of HAs from 13.5% (MnCuK-FeC alone) to 15.5%.Table 3

The *in-situ* DRIFT results in Figure 6 show that on the MnCuK-FeC and CuZnAlZr tandem catalyst, the intensity of the $*C_2H_5O$ species located at 2925 cm^{-1} and 2852 cm^{-1} is stronger than that on the single catalysts. This implies that mixing the two catalyst powders facilitates the formation of $*C_2H_5O$ during the hydrogenation of CO_2, indicating that the reaction process has a tendency to form long-chain oxygen-containing compounds (Lin et al., 2019; Xu et al., 2021) Therefore, we can conclude that by mixing the particles of MnCuK-FeC and CuZnAlZr to shorten the distance between the two components, the formation of long-chain oxygenated intermediates can be enhanced, thereby promoting the production of more HAs. Besides, the mixed catalyst of MnCuK-FeC and CuZnAlZr was able to maintain the stable Fe_5C_2 and metallic Cu phase states during 5 h on stream, as concluded from the *in-situ* XRD patterns (Figure 7). Both catalysts were able to maintain phase stability when tested individually, with MnCuK-FeC maintaining Fe_5C_2 and metallic

TABLE 3 Performance of CO_2 hydrogenation to higher alcohols.

Catalyst	T	GHSV	P	CO_2	HAs	Refs
	(°C)	(mL/h/g_{cat})	(MPa)	Conv. (%)	Sel. (%)	
MnCuK-FeC	300	6000	3	40.8	13.5	This Work
CuZnAlZr	300	6000	3	28.1	0	This Work
MnCuK-FeC(1)/ CuZnAlZr(1)	300	6000	3	42.1	15.5	This Work
FeC	300	6000	3	38.3	0	Huang et al. (2022)
Pt/Co_3O_4-r	200	6000	2	32.6	3.2	Nie et al. (2019)
Na-Co/SiO_2	250	4000	5	18.8	8.7	Nie et al. (2019)
CuZnK [a]	300	5000	6	25.1	3.96	Li et al. (2013)
CuZnK+CuFeCoK[a]	350	5000	6	32.4	6.54	Guo et al. (2014)
Co@Co_3O_4/C-N	220	6000	2	18.6	1.2	Nie et al. (2019)
LiRhMn/SiO_2	240	6000	5	16.1	7.7	Nie et al. (2019)

[a]Alcohol selectivity was based on wt%. Others were evaluated by C-mol%.
GHSV, Gas Hourly Space Velocity.

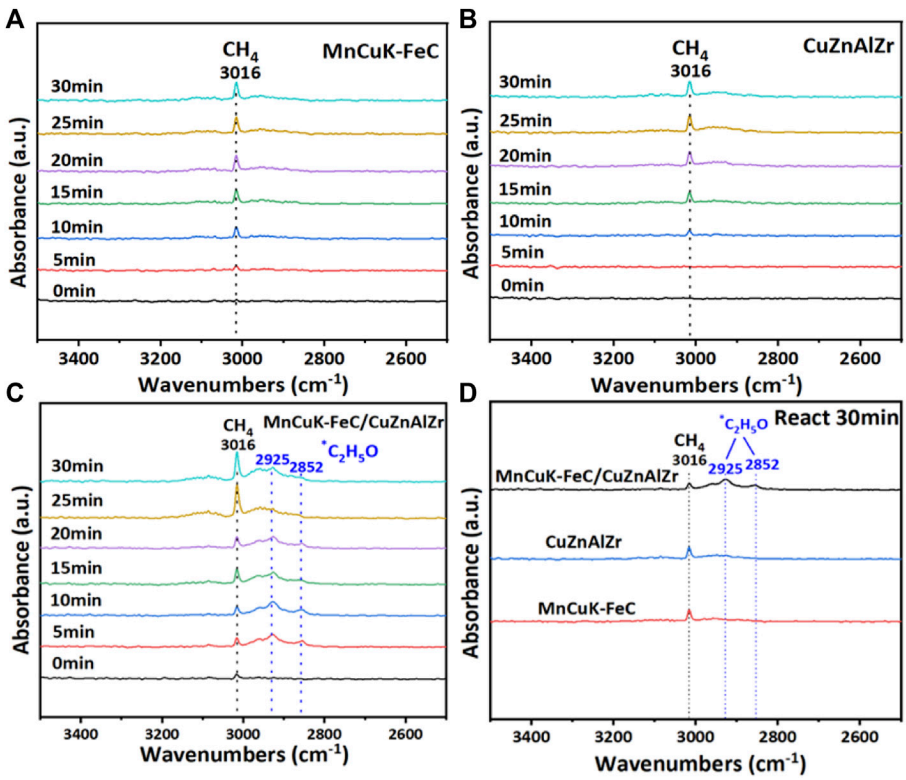

FIGURE 6
In-situ DRIFT spectra of CO_2+H_2 reaction over **(A)** MnCuK-FeC. **(B)** CuZnAlZr. **(C)** MnCuK-FeC/CuZnAlZr. **(D)** Comparison of the three catalysts after 30min reaction. (Reaction conditions: 15.0 ml/min H_2+5.0 ml/min CO_2, 1.0 MPa, 300°C).

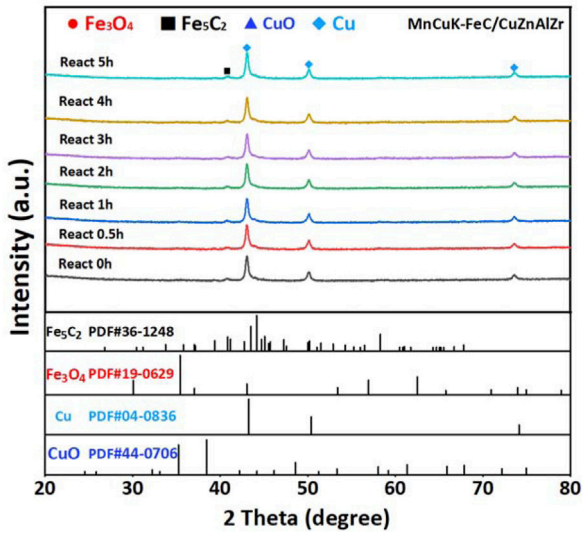

FIGURE 7
In-situ XRD patterns during reaction process of the MnCuK-FeC/CuZnAlZr catalyst. (1:1 powder mixing and filling).

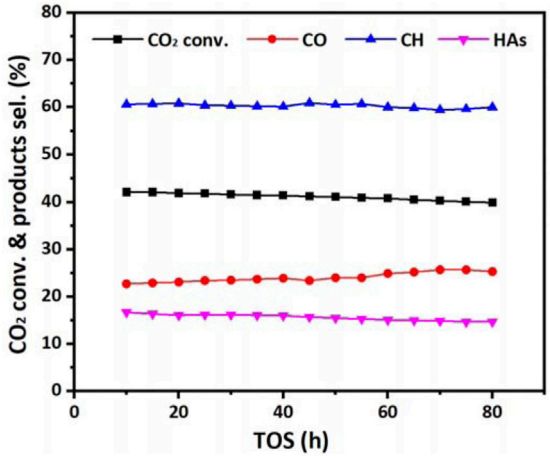

FIGURE 8
CO_2 conversion and product selectivity of MnCuK-FeC/CuZnAlZr in CO_2 hydrogenation during 80 h reaction. (Reaction Condition: H_2:CO_2=3:1, T = 300°C, p = 3 MPa, GHSV=6000 ml h^{-1}·g_{cat}^{-1}).

Cu and CuZnAlZr maintaining the metallic Cu phase state (Supplementary Figure S7 and S8).

It is also worth noting that no significant deactivation of the mixed catalyst was observed during 80 h of continuous reaction for the CO_2 hydrogenation, as shown in Figure 8.

4 Conclusion

In summary, we successfully prepared multifunctional catalysts composed of Mn, Cu, and K modified iron carbide and CuZnAlZr, which showed excellent activity and stability in the preparation of HAs by CO_2 hydrogenation. Meanwhile, the catalysts were evaluated by different loading methods and catalyst filling mass ratios, and it was found that the best performance was obtained by mixing the two components in a 1:1 mass ratio powder, and the selectivity of HAs in the product was 15.5%, which was a relatively significant improvement (7.6%–13%) compared to the layered loading and other mass ratios of catalyst combinations. In addition, the selectivity of propanol and butanol was about 40% of the HAs. The synergistic effect between the Mn-Cu-K modified iron carbide and CuZnAlZr fractions on the synthesis of HAs may result from the enhanced formation of $^*C_2H_5O$ intermediates and their further hydrogenation to form HAs. This work provides a promising approach for the preparation of multifunctional catalysts for more selective HAs formation via CO_2 hydrogenation.

Data availability statement

The original contributions presented in the study are included in the article/Supplementary Material, further inquiries can be directed to the corresponding authors.

Author contributions

JH performed the experimental design, samples preparation and testing and manuscript writing, JZ, MW, and FD revised the article, GZ reviewed and supervised the manuscript, CS and WX reviewed, edited, supervised the work, and obtained funding. All authors contributed to the article and approved the submitted version.

Funding

This work was financially supported by the Major Science and Technology Special Project of Xinjiang Uygur Autonomous Region (2022A01002-1), the Fundamental Research Funds for the Central Universities (DUT22LAB602), the Liaoning Revitalization Talent Program (XLYC2008032) and the CUHK Research Startup Fund (No.#4930981).

Acknowledgments

We acknowledge the Center for Advanced Mössbauer Spectroscopy, Mössbauer Effect Data Center, Dalian Institute

of Chemical Physics, CAS, for providing the Mössbauer measurement and analysis.

Conflict of interest

The authors declare that the research was conducted in the absence of any commercial or financial relationships that could be construed as a potential conflict of interest.

Publisher's note

Supplementary material

The Supplementary Material for this article can be found online at: https://www.frontiersin.org/articles/10.3389/fenrg.2022.995800/full#supplementary-material

References

Ahmed, M., Rüsing, M., Berth, G., Lischka, K., and Pawlis, A. (2013). CuO and Co_3O_4 nanoparticles: Synthesis, characterizations, and Raman spectroscopy. *J. Nanomater.* 2013, 714853. doi:10.1155/2013/714853

Ao, M., Pham, G. H., Sunarso, J., Tade, M. O., and Liu, S. (2018). Active centers of catalysts for higher alcohol synthesis from syngas: A review. *ACS Catal.* 8, 7025–7050. doi:10.1021/acscatal.8b01391

Bauer, A. (2018). ZrO_2 Phase identification with Raman spectroscopy. *Appl. Note Raman-020* 4, 01–03.

Behrens, M., Studt, F., Kasatkin, I., Kuhl, S., Havecker, M., Abild-Pedersen, F., et al. (2012). The active site of methanol synthesis over $Cu/ZnO/Al_2O_3$ industrial catalysts. *Science* 336, 893–897. doi:10.1126/science.1219831

Cao, A., Schumann, J., Wang, T., Zhang, L., Xiao, J., Bothra, P., et al. (2018). Mechanistic insights into the synthesis of higher alcohols from syngas on CuCo alloys. *ACS Catal.* 8, 10148–10155. doi:10.1021/acscatal.8b01596

Chang, H., Lin, Q., Cheng, M., Zhang, K., Feng, B., Chai, J., et al. (2022). Effects of potassium loading over iron–silica interaction, phase evolution and catalytic behavior of precipitated iron-based catalysts for fischer-tropsch synthesis. *Catalysts* 12, 916. doi:10.3390/catal12080916

Christensen, J. M., Mortensen, P. M., Trane, R., Jensen, P. A., and Jensen, A. D. (2009). Effects of H_2S and process conditions in the synthesis of mixed alcohols from syngas over alkali promoted cobalt-molybdenum sulfide. *Appl. Catal. A General* 366, 29–43. doi:10.1016/j.apcata.2009.06.034

Cosultchi, A., Pérez-Luna, M., Morales-Serna, J. A., and Salmón, M. (2012). Characterization of modified fischer–tropsch catalysts promoted with alkaline metals for higher alcohol synthesis. *Catal. Lett.* 142, 368–377. doi:10.1007/s10562-012-0765-9

Elango, M., Deepa, M., Subramanian, R., and Mohamed Musthafa, A. (2017). Synthesis, characterization, and antibacterial activity of polyindole/Ag–CuO nanocomposites by reflux condensation method. *Polymer-Plastics Technol. Eng.* 57, 1440–1451. doi:10.1080/03602559.2017.1410832

Gao, P., Zhang, L., Li, S., Zhou, Z., and Sun, Y. (2020). Novel heterogeneous catalysts for CO_2 hydrogenation to liquid fuels. *ACS Cent. Sci.* 6, 1657–1670. doi:10.1021/acscentsci.0c00976

Guo, H., Li, S., Peng, F., Zhang, H., Xiong, L., Huang, C., et al. (2014). Roles investigation of promoters in K/Cu–Zn catalyst and higher alcohols synthesis from CO_2 hydrogenation over a novel two-stage bed catalyst combination system. *Catal. Lett.* 145, 620–630. doi:10.1007/s10562-014-1446-7

Huang, J., Zhang, G., Zhu, J., Wang, M., Ding, F., Song, C., et al. (2022). Boosting the production of higher alcohols from CO_2 and H_2 over Mn- and K-modified iron carbide. *Ind. Eng. Chem. Res.* 61, 7266–7274. doi:10.1021/acs.iecr.2c00720

Iranmahboob, J., Toghiani, H., and Hill, D. O. (2003). Dispersion of alkali on the surface of Co-MoS_2/clay catalyst: A comparison of K and Cs as a promoter for synthesis of alcohol. *Appl. Catal. A General* 247, 207–218. doi:10.1016/s0926-860x(03)00092-9

Jayarambabu, N. (2014). Germination and growth characteristics of mungbean seeds (vigna radiata L.) affected by synthesized zinc oxide nanoparticles. *Int. J. Curr. Eng. Technol.* 4, 5.

Kangvansura, P., Chew, L. M., Kongmark, C., Santawaja, P., Ruland, H., Xia, W., et al. (2017). Effects of potassium and manganese promoters on nitrogen-doped carbon nanotube-supported iron catalysts for CO_2 hydrogenation. *Engineering* 3, 385–392. doi:10.1016/j.eng.2017.03.013

Kangvansura, P., Chew, L. M., Saengsui, W., Santawaja, P., Poo-arporn, Y., Muhler, M., et al. (2016). Product distribution of CO_2 hydrogenation by K- and Mn-promoted Fe catalysts supported on N -functionalized carbon nanotubes. *Catal. Today* 275, 59–65. doi:10.1016/j.cattod.2016.02.045

Lee, J. H., Lee, H.-K., Kim, K., Rhim, G. B., Youn, M. H., Jeong, H., et al. (2021). Unravelling the K-promotion effect in highly active and stable Fe_5C_2 nanoparticles for catalytic linear α-olefin production. *Mat. Adv.* 2, 1050–1058. doi:10.1039/d0ma00920b

Li, S., Guo, H., Luo, C., Zhang, H., Xiong, L., Chen, X., et al. (2013). Effect of iron promoter on structure and performance of K/Cu–Zn catalyst for higher alcohols synthesis from CO_2 hydrogenation. *Catal. Lett.* 143, 345–355. doi:10.1007/s10562-013-0977-7

Liang, B., Ma, J., Su, X., Yang, C., Duan, H., Zhou, H., et al. (2019). Investigation on deactivation of $Cu/ZnO/Al_2O_3$ catalyst for CO_2 hydrogenation to methanol. *Ind. Eng. Chem. Res.* 58, 9030–9037. doi:10.1021/acs.iecr.9b01546

Lin, T., Qi, X., Wang, X., Xia, L., Wang, C., Yu, F., et al. (2019). Direct production of higher oxygenates by syngas conversion over a multifunctional catalyst. *Angew. Chem. Int. Ed. Engl.* 58, 4675–4679. doi:10.1002/ange.201814611

Liu, J., Sun, Y., Jiang, X., Zhang, A., Song, C., and Guo, X. (2018). Pyrolyzing ZIF-8 to N-doped porous carbon facilitated by iron and potassium for CO_2 hydrogenation to value-added hydrocarbons. *J. CO_2 Util.* 25, 120–127. doi:10.1016/j.jcou.2018.03.015

Liu, J., Zhang, A., Jiang, X., Zhang, G., Sun, Y., Liu, M., et al. (2019). Overcoating the surface of Fe-based catalyst with ZnO and nitrogen-doped carbon toward high selectivity of light olefins in CO_2 hydrogenation. *Ind. Eng. Chem. Res.* 58, 4017–4023. doi:10.1021/acs.iecr.8b05478

Liu, J., Zhang, G., Jiang, X., Wang, J., Song, C., and Guo, X. (2021). Insight into the role of Fe_5C_2 in CO_2 catalytic hydrogenation to hydrocarbons. *Catal. Today* 371, 162–170. doi:10.1016/j.cattod.2020.07.032

Liu, X., Cao, C., Tian, P., Zhu, M., Zhang, Y., Xu, J., et al. (2020). Resolving CO_2 activation and hydrogenation pathways over iron carbides from DFT investigation. *J. CO_2 Util.* 38, 10–15. doi:10.1016/j.jcou.2019.12.014

Liu, Y., Cheng, B., Wang, K. K., Ling, G. P., Cai, J., Song, C. L., et al. (2014). Study of Raman spectra for γ-Al_2O_3 models by using first-principles method. *Solid State Commun.* 178, 16–22. doi:10.1016/j.ssc.2013.09.030

Liu, Y., Murata, K., and Inaba, M. (2014). Synthesis of mixed alcohols from synthesis gas over alkali and Fischer–Tropsch metals modified MoS_2/Al_2O_3-montmorillonite catalysts. *Reac. Kinet. Mech. Cat.* 113, 187–200. doi:10.1007/s11144-014-0725-z

Luk, H. T., Mondelli, C., Ferre, D. C., Stewart, J. A., and Perez-Ramirez, J. (2017). Status and prospects in higher alcohols synthesis from syngas. *Chem. Soc. Rev.* 46, 1358–1426. doi:10.1039/C6CS00324A

Mironova-Ulmane, N., Kuzmin, A., Skvortsova, V., Chikvaidze, G., Sildos, I., Grabis, J., et al. (2018). Synthesis and vibration spectroscopy of nano-sized

manganese oxides. *Acta Phys. Pol. A* 133, 1013–1016. doi:10.12693/aphyspola.133.1013

Naayi, S., Hassan, A., and Salim, E. (2018). FTIR and X-ray diffraction analysis of Al_2O_3 nanostructured thin film prepared at low temperature using spray pyrolysis method. *Int. J. Nanoelectron. Mater.* 11, 1–6.

Nie, X., Li, W., Jiang, X., Guo, X., and Song, C. (2019). Recent advances in catalytic CO_2 hydrogenation to alcohols and hydrocarbons. *Adv. Catal.* 65, 121–233. doi:10.1016/bs.acat.2019.10.002

Ning, X., An, Z., and He, J. (2016). Remarkably efficient CoGa catalyst with uniformly dispersed and trapped structure for ethanol and higher alcohol synthesis from syngas. *J. Catal.* 340, 236–247. doi:10.1016/j.jcat.2016.05.014

Portillo Crespo, M. A., Villanueva Perales, A. L., Vidal-Barrero, F., and Campoy, M. (2015). Effects of methanol co-feeding in ethanol synthesis from syngas using alkali-doped MoS_2 catalysts. *Fuel Process. Technol.* 134, 270–274. doi:10.1016/j.fuproc.2015.02.006

Tada, S., Oshima, K., Noda, Y., Kikuchi, R., Sohmiya, M., Honma, T., et al. (2019). Effects of Cu precursor types on the catalytic activity of Cu/ZrO_2 toward methanol synthesis via CO_2 hydrogenation. *Ind. Eng. Chem. Res.* 58, 19434–19445. doi:10.1021/acs.iecr.9b03627

Temvuttirojn, C., Poo-arporn, Y., Chanlek, N., Cheng, C. K., Chong, C. C., Limtrakul, J., et al. (2020). Role of calcination temperatures of ZrO_2 support on methanol synthesis from CO_2 hydrogenation at high reaction temperatures over ZnO_x/ZrO_2 catalysts. *Ind. Eng. Chem. Res.* 59, 5525–5535. doi:10.1021/acs.iecr.9b05691

Tienthao, N., Hassanzahediniaki, M., Alamdari, H., and Kaliaguine, S. (2007). Effect of alkali additives over nanocrystalline Co–Cu-based perovskites as catalysts for higher-alcohol synthesis. *J. Catal.* 245, 348–357. doi:10.1016/j.jcat.2006.10.026

Wang, Y., Wang, K., Zhang, B., Peng, X., Gao, X., Yang, G., et al. (2021). Direct conversion of CO_2 to ethanol boosted by intimacy-sensitive multifunctional catalysts. *ACS Catal.* 11, 11742–11753. doi:10.1021/acscatal.1c01504

Wu, Q., Shen, C., Rui, N., Sun, K., and Liu, C. J. (2021). Experimental and theoretical studies of CO_2 hydrogenation to methanol on Ru/In_2O_3. *J. CO_2 Util.* 53, 101720. doi:10.1016/j.jcou.2021.101720

Xu, D., Ding, M., Hong, X., and Liu, G. (2020). Mechanistic aspects of the role of K promotion on Cu–Fe-based catalysts for higher alcohol synthesis from CO_2 hydrogenation. *ACS Catal.* 10, 14516–14526. doi:10.1021/acscatal.0c03575

Xu, D., Ding, M., Hong, X., Liu, G., and Tsang, S. C. E. (2020). Selective C_{2+} alcohol synthesis from direct CO_2 hydrogenation over a Cs-promoted Cu-Fe-Zn catalyst. *ACS Catal.* 10, 5250–5260. doi:10.1021/acscatal.0c01184

Xu, D., Yang, H., Hong, X., Liu, G., and Edman Tsang, S. C. (2021). Tandem catalysis of direct CO_2 hydrogenation to higher alcohols. *ACS Catal.* 11, 8978–8984. doi:10.1021/acscatal.1c01610

Yang, C., Liu, S., Wang, Y., Song, J., Wang, G., Wang, S., et al. (2019). The interplay between structure and product selectivity of CO_2 hydrogenation. *Angew. Chem. Int. Ed. Engl.* 58, 11242–11247. doi:10.1002/anie.201904649

Yang, Y., Lin, T., Qi, X., Yu, F., An, Y., Li, Z., et al. (2018). Direct synthesis of long-chain alcohols from syngas over CoMn catalysts. *Appl. Catal. A General* 549, 179–187. doi:10.1016/j.apcata.2017.09.037

Zeng, F., Mebrahtu, C., Xi, X., Liao, L., Ren, J., Xie, J., et al. (2021). Catalysts design for higher alcohols synthesis by CO_2 hydrogenation: Trends and future perspectives. *Appl. Catal. B* 2021, 291. doi:10.1016/j.apcatb.2021.120073

Zhang, F., Zhou, W., Xiong, X., Wang, Y., Cheng, K., Kang, J., et al. (2021). Selective hydrogenation of CO_2 to ethanol over sodium-modified rhodium nanoparticles embedded in zeolite silicalite-1. *J. Phys. Chem. C* 125, 24429–24439. doi:10.1021/acs.jpcc.1c07862

Zhao, B., Liu, Y., Zhu, Z., Guo, H., and Ma, X. (2018). Highly selective conversion of CO_2 into ethanol on $Cu/ZnO/Al_2O_3$ catalyst with the assistance of plasma. *J. CO_2 Util.* 24, 34–39. doi:10.1016/j.jcou.2017.10.013

Zhao, Z., Lu, W., Yang, R., Zhu, H., Dong, W., Sun, F., et al. (2017). Insight into the formation of $Co@Co_2C$ catalysts for direct synthesis of higher alcohols and olefins from syngas. *ACS Catal.* 8, 228–241. doi:10.1021/acscatal.7b02403

Zheng, M., Zhang, H., Gong, X., Xu, R., Xiao, Y., Dong, H., et al. (2013). A simple additive-free approach for the synthesis of uniform manganese monoxide nanorods with large specific surface area. *Nanoscale Res. Lett.* 8, 166. doi:10.1186/1556-276x-8-166

Zhu, J., Wang, P., Zhang, X., Zhang, G., Li, R., Li, W., et al. (2022). Dynamic structural evolution of iron catalysts involving competitive oxidation and carburization during CO_2 hydrogenation. *Sci. Adv.* 8, eabm3629. doi:10.1126/sciadv.abm3629

Zhu, J., Zhang, G., Li, W., Zhang, X., Ding, F., Song, C., et al. (2020). Deconvolution of the particle size effect on CO_2 hydrogenation over iron-based catalysts. *ACS Catal.* 10, 7424–7433. doi:10.1021/acscatal.0c01526

Zhuo, R., Feng, H., Liang, Q., Liu, J., Chen, J., Yan, D., et al. (2008). Morphology-controlled synthesis, growth mechanism, optical and microwave absorption properties of ZnO nanocombs. *J. Phys. D. Appl. Phys.* 41, 185405–185413. doi:10.1088/0022-3727/41/18/185405